Mineralogical Magazine, December 2007, Vol. 71(6), pp. 683–690

Crystal structure and crystal chemistry of fluorannite and its relationships to annite

M. F. Brigatti[1]*, E. Caprilli[2], D. Malferrari[1] and A. Mottana[2]

[1] Dipartimento di Scienze della Terra, Università di Modena e Reggio Emilia, Modena, Italy
[2] Dipartimento di Scienze Geologiche, Università degli Studi Roma Tre, Roma, Italy

[*Received 21 January 2008; Accepted 11 April 2008*]

ABSTRACT

This study focuses on the crystal-chemical characterization of fluorannite from the Katugin Ta-Nb deposit, Chitinskaya Oblast', Kalar Range, Transbaikalia, eastern Siberia, Russia. The chemical formula of this mineral is $(K_{0.960}Na_{0.020}Ba_{0.001})(Fe^{2+}_{2.102}Fe^{3+}_{0.425}Cr^{3+}_{0.002}Mg_{0.039}Li_{0.085}Ti_{0.210}Mn_{0.057})(Al_{0.674}Si_{3.326})O_{10}(F_{1.060}OH_{0.028}O_{0.912})$. This mica belongs to the 1*M* polytype (space group *C*2/*m*) with layer parameters a = 5.3454(2) Å, b = 9.2607(4) Å, c = 10.2040(5) Å, β = 100.169(3)º. Structure refinement, using anisotropic displacement parameters, converged at R = 0.0384. When compared to annite, fluorannite shows a smaller cell volume ($V_{fluorannite}$ = 497.19 Å^3; V_{annite} = 505.71 Å^3), because of its smaller lateral dimensions and c parameter. Flattening in the plane of the tetrahedral basal oxygen atoms decreases with F content, together with the A–O4 distance (i.e. the distance between interlayer cation A and the octahedral anionic position) due to the reduced repulsion between the interlayer cation and the anion sited in O4.

Keywords: fluorannite, trioctahedral mica, crystal structure, Katugin, Russia.

Introduction

Fluorannite was described as a new trioctahedral mica by Shen *et al*. (2000). The chemical composition, crystal data, and Mössbauer and infrared spectroscopy (IR) data for the fluorannite holotype occurring in the A-type granite pluton of Suzhou, eastern China (Shen, 2002) were published recently by Shen *et al*. (2000, 2002). The mineral crystallizes as 1*M* polytype (space group *C*2/*m*) with unit-cell parameters a = 5.369(8) Å, b = 9.289(3) Å, c = 10.153(8) Å and β = 100.49(1)º, and has the following chemical formula: $(K_{0.92}Na_{0.03}Rb_{0.02}Ba_{0.01})(Fe^{2+}_{1.82}Fe^{3+}_{0.49}Al_{0.19}Mg_{0.18}Li_{0.16}Ti_{0.08}Mn_{0.05}Zn_{0.02})(Al_{1.17}Si_{2.83})O_{10}(F_{1.03}OH_{0.50}O_{0.47})$. Mössbauer spectroscopy suggests that both Fe^{2+} and Fe^{3+} occupy the octahedral sites with a prevalence of Fe^{2+}.

Fluorine can substitute for OH in micas, following a mechanism which enhances the stability of the trioctahedral mica structure. In addition, the extent of this substitution depends on several factors: (1) hydrofluoric activity during crystallization and post-crystallization events; (2) crystallization temperature; and (3) octahedral sheet population and occupancy, with a strong preference for trioctahedral Mg-rich micas (Munoz, 1984; Mason, 1992; Robert *et al*., 1993; Papin *et al*., 1997; Boukili *et al*., 2001, 2002; Fechtelkord *et al*., 2003*a*,*b*).

Natural trioctahedral micas were investigated intensively by single-crystal X-ray diffraction (XRD) methods (Brigatti and Guggenheim, 2002); however, studies on Fe-rich micas are rare. At present, the Fe-bearing micas closest to the annite ideal composition were studied by Brigatti *et al.* (2000*a*), who characterized an annite from Pikes Peak (Colorado), and by Redhammer and Roth (2002), who provided crystal structure refinements for an annite from Mont Saint-Hilaire (Québec), first addressed by Lalonde *et al.* (1996),

* E-mail: brigatti@unimore.it
DOI: 10.1180/minmag.2007.071.6.683

with relevant tetrahedral Fe^{3+} content. Studies on other trioctahedral micas with compositions close to annite, but with relevant Al contents, were also reported by Brigatti *et al.* (2000*b*). In addition to natural trioctahedral micas, Redhammer and Roth (2002, 2004) studied a variety of synthetic Fe-rich samples with various octahedral contents, but containing no fluorine. Other structural studies of Fe, OH-rich micas were carried out for Cs-tetra-ferri-annite (Mellini *et al.*, 1996; Comodi *et al.*, 1999) and for Rb-tetra-ferri-annite (Comodi *et al.*, 2003).

This study attempts to: (1) characterize the crystal structure of F-rich annite from the Katugin Ta-Nb deposit, Russia; (2) compare its crystal chemistry with that of OH-rich annite from the Pikes Peak complex, Colorado, USA; and (3) verify the influence of the F-for-OH substitution on the layer.

Experimental

Samples

The studied fluorannite was found in the Katugin deposit, Chitinskaya Oblast', Kalar Range, Transbaikalia, eastern Siberia, Russia. The deposit consists of a Ta-, Nb- and *REE*-bearing alkaline metasomatite, which replaces multistage alkali-*REE* granites and host-rocks that are generally composed of marble, gneiss or amphibolite. The deposit comprises fine- and medium-grained quartz-albite-microcline rocks. Ta-Ni minerals, zircon and thorite are widespread along with *REE* minerals (e.g. gagarinite, yttrofluorite, monazite, bastnäsite and xenotime). The depositional environment consists of deposit-hosting intrusions and metasomatic deposits which occur along major shear zones connected to intraplate and continental-margin rift and strike-slip faults (Solodov *et al.*, 1987; Kremenetsky *et al.*, 2000).

The annite from the Pikes Peak batholith (central Colorado) was used to assess the influence of the anionic position on layer topology. Although the chemical and structural data for this sample had been previously reported (Brigatti *et al.*, 2000*a*), we collected all the data again using the same experimental set-up used to characterize fluorannite.

Chemical composition

Major-element composition of the crystals used for structure refinement were obtained by wavelength-dispersive spectroscopic (WDS) methods using an ARL-SEMQ electron microprobe (EMP) at the Dipartimento di Scienze della Terra, Università di Modena e Reggio Emilia. Analyses were performed with a 15 kV accelerating voltage, 15 nA beam current and a 5−10 μm beam-spot diameter. Different counting times were employed, both at peak and background positions: 10 s for Na, 15 s for K, Si, Fe, Mn, Al, Mg, Ca and Ti, and 40 s for F, as suggested by Signorelli *et al.* (1999). The following standards were used: fluorite (F); microcline (K); albite (Na); spessartine (Al,Mn); ilmenite (Fe,Ti); clinopyroxene (Si); olivine (Mg). Analysis and data reduction were performed using the Probe software package of Donovan (1995). The $(OH)^-$ content of annite was measured by thermogravimetric analysis (TGA) in He gas flow using a Seiko SSC 5200 thermal analyser (heating rate 10ºC/min; gas-flow rate 100 μl/min), equipped with a mass spectrometer (GeneSys ESS, Quadstar 422). A similar approach was unsuitable for fluorannite due to the limited amount of available material.

The compositions reported in Table 1 were obtained by combining the average of at least seven EMP point-analyses with information related to single-crystal structure refinement (i.e. comparing the mean electron count of interlayer and octahedral cation sites obtained from chemical analysis with those from single-crystal structure refinement). Further information taken into consideration for the derivation of the chemical formula includes: (1) $(OH)^-$ determination on several annite crystals selected from the same sample containing the crystal used for structure refinement; and (2) information related to Fe-oxidation state as indicated for fluorannite by Shen *et al.* (2002). The chemical formula is based on $O_{12-x-y-z}(OH)_xF_yCl_z$.

XRD analysis

Small crystal fragments of fluorannite from the Katugin deposit (crystal size: 0.130 mm × 0.105 mm × 0.015 mm) and annite from the Pikes Peak batholith (0.125 mm × 0.100 mm × 0.010 mm) were analysed using a Bruker AXS X8 APEX automated diffractometer with a four circle Kappa goniometer, an APEX 4K CCD detector, flat graphite monochromator and Mo-$K\alpha$-radiation (λ = 0.71073 Å) from a fine focus sealed tube. Three sets of 12 frames were used for the initial unit-cell determination; each frame

TABLE 1. Chemical data for fluorannite and annite. The standard deviations of seven point analyses are reported in parentheses.

Sample	Fluorannite	Annite		Fluorannite	Annite
(wt.%)			(a.p.f.u.)		
SiO_2	39.21(0.81)	36.95(0.86)	Si	3.326	3.147
TiO_2	3.30(0.05)	3.5(0.08)	Al	0.674	0.853
Al_2O_3	6.74(0.12)	9.25(0.20)	$\Sigma_{T\ site}$	4.000	4.000
Cr_2O_3	0.03(0.01)	b.d.l.	Al		0.075
Fe_2O_3*	6.66	3.38	Ti	0.210	0.224
FeO	29.64(0.20)	31.93(0.28)	Cr	0.002	
MnO	0.80(0.04)	0.51(0.05)	Fe^{3+}	0.425	0.217
MgO	0.31(0.02)	1.06(0.05)	Fe^{2+}	2.102	2.274
Li_2O	0.25(0.06)	0.11(0.05)	Mn	0.057	0.037
Na_2O	0.12(0.03)	0.02(0.01)	Mg	0.039	0.135
K_2O	8.87(0.31)	9.17(0.28)	Li	0.085	0.038
BaO	0.02(0.01)	b.d.l.	$\Sigma_{M\ sites}$	2.920	3.000
F	3.95(0.34)	0.99(0.26)	Na	0.020	0.003
Cl		0.05(0.02)	K	0.960	0.996
H_2O	0.10**	3.10	Ba	0.001	
Sum	100.00	100.02	$\Sigma_{A\ site}$	0.981	0.999
O = F, Cl	−1.66	−0.43	F	1.060	0.267
			OH	0.028	0.880
			Cl		0.007
			O	10.912	10.846
			Σ	12.000	12.000

* Calculated according to Mössbauer suggestions obtained on fluorannite from Suzhou (Shen *et al*., 2002) and crystal structure refinement.
** Calculated
b.d.l.: below detection limit

measured with 0.5º φ rotation and 10 s exposure time. The crystal–detector distance was 40 mm and the collection strategy was optimized by the APEX program suite (Bruker, 2003*a*). The refined cell parameters are a = 5.3454(2) Å, b = 9.2607(4) Å, c = 10.2040(5) Å, β = 100.169(3)º, V = 497.19 Å^3 for fluorannite, and a = 5.3841(1) Å, b = 9.3259(3) Å, c = 10.2549(3) Å, β = 100.851(1)º, V = 505.71 Å^3 for annite. The whole Ewald sphere (±9 h, ±16 k, ±18 l) was recorded in the range 4º < θ < 41º. A total of 6217 reflections (unique reflections: 1559; R_{int}: 0.0386) and 5685 reflections (unique reflections: 1359; R_{int}: 0.0303) were collected for fluorannite and annite, respectively. A semi-empirical absorption collection based on the intensity of equivalent reflections was applied using the SADABS software (Sheldrick, 2003). The SAINT-IRIX (Bruker, 2003*b*) package was used for data reduction and unit-cell refinement. Anisotropic crystal-structure refinement was carried out using the SHELX-97 package of programs (Sheldrick, 1997) in the monoclinic space group $C2/m$ with neutral atomic scattering factors and starting from the previously determined atomic coordinates of annite (Brigatti *et al.*, 2000*a*). These methods finally led to the positional and displacement parameters for all atoms reported in Table 2. Ionized X-ray scattering curves were employed for non-tetrahedral cations, whereas ionized *vs.* neutral species were used for Si and O (Hawthorne *et al.*, 1995). The final refinement yielded the following agreement factors: R = 0.0384 and R = 0.0398 for fluorannite and annite, respectively. A final calculated difference electron density (DED) map did not reveal significant excess in electron density above the background. Table 3 reports relevant cation-anion bond lengths, the mean electron count at the octahedral and interlayer sites, and selected parameters derived from structure refinement. The observed and calculated structure factors can be requested directly from the authors.

TABLE 2. Crystallographic coordinates and equivalent isotropic displacement parameters ($Å^2 \times 10^3$). $U_{(eq)}$ is defined as one third of the trace of the orthogonalized *Uij* tensor.

	x	*y*	*z*	$U_{(eq)}$	U_{11}	U_{22}	U_{33}	U_{23}	U_{13}	U_{12}
Fluorannite, 1*M* polytype (space group: *C*2/*m*)										
O1	0.0515(4)	0	0.1651(2)	21(1)	27(1)	15(1)	19(1)	0	2(1)	0
O2	0.3062(2)	0.2487(2)	0.1651(1)	20(1)	17(1)	27(1)	17(1)	−2(1)	3(1)	−7(1)
O3	0.1294(2)	0.1668(1)	0.3878(1)	12(1)	11(1)	14(1)	11(1)	0(1)	2(1)	0(1)
O4	0.1287(3)	0.5	0.3924(2)	21(1)	18(1)	21(1)	23(1)	0	3(1)	0
T	0.0744(1)	0.1666(1)	0.2240(1)	9(1)	8(1)	9(1)	11(1)	0(1)	1(1)	0(1)
*M*1	0	0	0.5	11(1)	10(1)	10(1)	13(1)	0	4(1)	0
*M*2	0	0.3338(1)	0.5	11(1)	8(1)	12(1)	12(1)	0	1(1)	0
A	0	0.5	0	34(1)	29(1)	32(1)	42(1)	0	6(1)	0
Annite, 1*M* polytype (space group: *C*2/*m*)										
O1	0.0395(4)	0	0.1679(2)	22(1)	33(1)	15(1)	16(1)	0	3(1)	0
O2	0.3022(3)	0.2461(2)	0.1668(1)	21(1)	18(1)	29(1)	16(1)	−2(1)	3(1)	−8(1)
O3	0.1290(3)	0.1676(1)	0.3897(1)	14(1)	14(1)	15(1)	12(1)	0(1)	2(1)	0(1)
O4	0.1260(4)	0.5	0.3943(2)	26(1)	22(1)	24(1)	32(1)	0	5(1)	0
T	0.0691(1)	0.1668(1)	0.2243(1)	11(1)	10(1)	11(1)	13(1)	0(1)	2(1)	0(1)
*M*1	0	0	0.5	12(1)	11(1)	10(1)	16(1)	0	4(1)	0
*M*2	0	0.3336(1)	0.5	13(1)	9(1)	14(1)	15(1)	0	2(1)	0
A	0	0.5	0	44(1)	37(1)	41(1)	50(1)	0	1(1)	0

Results and discussion

The chemical composition of fluorannite from the Katugin Ta-Nb deposit is $(K_{0.960}Na_{0.020}Ba_{0.001})(Fe^{2+}_{2.102}Fe^{3+}_{0.425}Cr^{3+}_{0.002}Mg_{0.039}Li_{0.085}Ti_{0.210}Mn_{0.057})(Al_{0.674}Si_{3.326})O_{10}(F_{1.060}OH_{0.028}O_{0.912})$ (Table 1).

When compared to annite, fluorannite shows a smaller cell volume ($V_{fluorannite}$ = 497.19 $Å^3$; V_{annite} = 505.71 $Å^3$), because of its smaller lateral dimensions and *c* parameter (*c* = 10.2040(5) Å and *c* = 10.2549(3) Å for fluorannite and annite, respectively). According to Robert *et al.* (1993), F enters the mica structure in the octahedral anionic site substituting for OH. Hence the reduction in the *c* parameter can be attributed to the electrostatic interaction of the interlayer cation on the anionic site, which is obviously greater when F substitutes for the OH group. This effect is particularly clear in trioctahedral micas, where OH points directly towards the interlayer cation, rather than being inclined towards the empty octahedral site, as in dioctahedral micas. The interlayer separation also decreases: from 3.375 Å in annite to 3.316 Å in fluorannite (Table 3).

In fluorannite, Si and Al occupy the tetrahedral site in a ratio Si/(Si+Al) = 0.83. The site volume is 2.307(1) A^3. The $\langle T{-}O\rangle$ mean bond distance ($\langle T{-}O\rangle$ = 1.651 Å) is slightly shorter than in annite ($\langle T{-}O\rangle$ = 1.660 Å), but very close to the value measured for fluorphlogopite ($\langle T{-}O\rangle$ = 1.648 Å, Gianfagna *et al.*, 2007). The tetrahedral cation is displaced towards the apical oxygen atom, thus also accounting for a slightly smaller tetrahedral-cation–apical-oxygen-atom distance than the tetrahedral-cation–basal-oxygen-atom distances (Table 3). A further consequence is the increase of the O_{basal}–T–O_{apical} angles (i.e. τ parameter = 110.97°). Furthermore, the basal tetrahedral area in fluorannite (3.094 $Å^2$) is appreciably smaller than in annite (3.141 $Å^2$). All these effects can also be related to the large Si content, which, together with the high-charge octahedral cations, contributes to charge-balance the anionic O-for-OH substitutions.

In addition to the tetrahedral flattening angle, τ, tetrahedral distortion parameters commonly considered in micas are the in-plane rotation angle, α, and the corrugation of the basal oxygen atoms plane, Δ*z*. Both the α and Δ*z* parameters reflect mechanisms to fit tetrahedral and octahedral sheets together; in particular, α is the most effective mechanism to fit tetrahedral and octahedral sheets with different lateral dimensions, whereas Δ*z* increases when tetrahedral apical oxygen atoms link octahedral sites that are different in size. Fluorannite shows a very small in-plane rotation angle (α = 0.57°); smaller than in annite (α = 1.64°), and the tetrahedral basal oxygen atoms are completely in-plane (Δ*z* = 0.000). Hence, the α and Δ*z* parameters suggest

TABLE 3. Selected bond lengths (Å), mean electron count (m.e.c.) and parameters derived from structure refinement.

Sample	Fluorannite	Annite		Fluorannite	Annite
Tetrahedral sheet					
T−O1	1.6524(7)	1.6570(8)	α (°)	0.57	1.64
T−O2	1.651(1)	1.658(1)	Δ*z* (Å)	0.000	0.011
T−O2′	1.654(1)	1.660(1)	τ (°)	110.97	110.31
T−O3	1.645(1)	1.666(2)	*T*−O1⊥(001) (Å)	0.592	0.568
<*T*−O>	1.651	1.660	*T*−O3⊥(001) (Å)	1.645	1.666
			Sheet thickness (Å)	2.237	2.241
			Basal area (Å^2)	3.094	3.141
Octahedral sheet					
*M*1−O3 (×4)	2.111(1)	2.122(1)	Ψ_{M1} (°)	58.12	58.80
*M*1−O4 (×2)	2.092(1)	2.100(2)	Ψ_{M2} (°)	58.02	58.51
<*M*1−O>	2.105	2.115	m.e.c.$_{M1}$	25.6(1)	24.9(1)
			m.e.c.$_{M2}$	23.3(1)	24.2(1)
*M*2−O3 (×2)	2.106(1)	2.102(2)	*M*1−O4$_{[001]}$(°)	58.9	58.5
*M*2−O3′ (×2)	2.113(1)	2.111(1)	*M*2−O4$_{[001]}$(°)	58.6	59.2
*M*2−O4 (×2)	2.077(1)	2.078(1)	σ(O3−O3) (Å)	0.002	0.012
<*M*2−O>	2.099	2.097	σ(*M*−O) (Å)	0.013	0.015
			*M*2−O4−*M*2	99.8(1)	101.0(1)
			Sheet thickness (Å)	2.223	2.191
Interlayer					
A−O1 (×2)	3.127(2)	3.085(2)	<*A*−O>$_{inner}$	3.133	3.138
A−O1′ (×2)	3.164(2)	3.274(2)	<*A*−O>$_{outer}$	3.159	3.213
A−O2 (×4)	3.136(1)	3.164(2)	Δ(*A*−O) (Å)	0.026	0.075
A−O2′ (×4)	3.156(1)	3.183(2)	m.e.c. *A*	18.8(1)	19.3(1)
A−O4 (×2)	3.941(1)	3.972(2)	Sheet thickness (Å)	3.316	3.375

α (tetrahedral rotation angle) = $\sum_{i=1}^{6} \alpha_i/6$ where $\alpha_i = |120^o - \phi_i|/2$ and where ϕ_i is the angle between the basal edges of neighbouring tetrahedra articulated in the ring. $\Delta z = [Z_{(O_{basal})max} - Z_{(O_{basal})min}]$ [csinβ]. τ (tetrahedral flattening angle) = $\sum_{i=1}^{3}(O_{basal} - \hat{T} - O_{basal})_i/3$. ψ (octahedral flattening angle) = $\cos^{-1}$ [octahedral thickness/(2<*M*−O>)] (Donnay *et al*., 1964). *M*1−O4$_{[001]}$ and *M*2−O4$_{[001]}$ are the angles formed by *M*1−O4 and *M*2−O4 bonds with [001]. σ(O3−O3) is the variation between the lengths of O3−O3 octahedral edges. Overlapped-area$_{(001)}$ is the overlap of the areas defined between the two adjacent tetrahedral rings projected on (001).

that in fluorannite the tetrahedral and octahedral sheets, as well as each octahedron (*M*1 and *M*2), are very similar in size. Another implication of tetrahedral rotation angle being close to zero is an almost regular twelve-fold interlayer coordination.

The octahedral sites are mainly occupied by Fe, with minor amounts of Ti, Mg and Li. The mean bond distance of *M*1 (⟨*M*1−O⟩ = 2.105 Å) and *M*2 sites (⟨*M*2−O⟩ = 2.099 Å) as well as the flattening angles Ψ (Ψ_{M1} = 58.12°; Ψ_{M2} = 58.02°) and the mean electron count at *M*1 and *M*2 (m.e.c.$_{M1}$ = 25.6; m.e.c.$_{M2}$ = 23.3) confirm a slight preference of the largest and heaviest cations for *M*1. The octahedral thickness (2.223 Å) is greater than in annite (2.191 Å).

To better characterize the impact of F-for-OH substitution onto the layer topology, we selected a dataset (Brigatti *et al*., 2000*b*; Redhammer and Roth, 2002) of natural crystals close to the annite end-member ($^{[VI]}Fe_{tot} \geqslant 1.5$ a.p.f.u.) with variable F-for-OH and O-for-OH substitutions. The F content in our dataset appears to be a powerful crystal-chemical indicator driving numerous structural parameters. In particular, Δ*z* decreases with F content (Fig. 1*a*), together with the *A*−O4 distance (i.e. the distance between interlayer *A* cation and the octahedral anionic position, Fig. 1*b*). There is an immediate crystal-chemical interpretation for the trend in Fig. 1*b*, since the repulsive *A*−H interaction is progressively

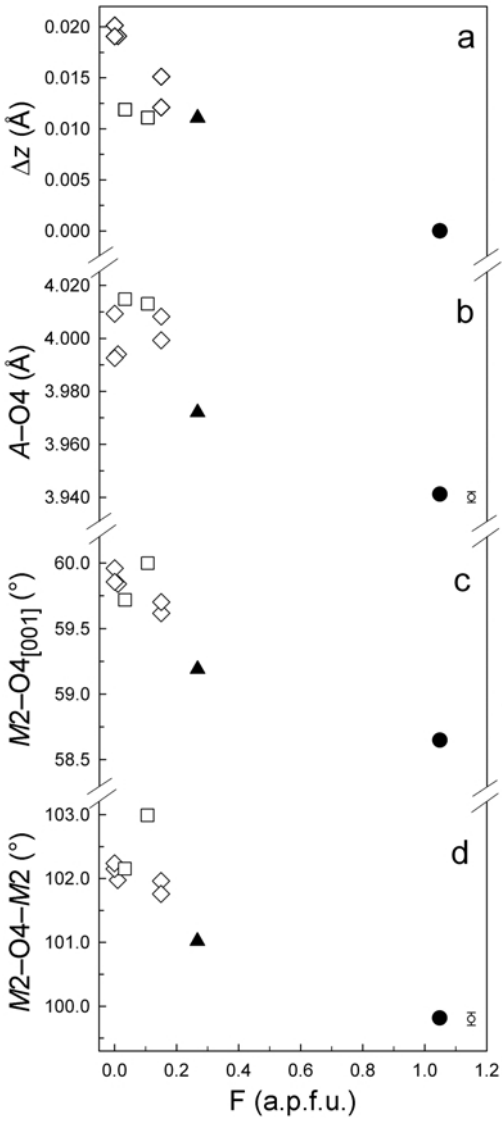

FIG. 1. Variation of F content with the following structural parameters: (*a*) Δz (flattening of the basal oxygen plane); (*b*) $A-$O4 (distance between interlayer cation (A) and octahedral anionic position (O4)); (*c*) $M2-O4_{[001]}$ (i.e. projection on [001] of the distance between the octahedral $M2$ cation and the O4 oxygen atom); and (*d*) $M2$-$\hat{O}4$-$M2$ angle. Legend: filled circle – fluorannite; filled triangle – annite; open symbols – samples from the literature (diamond: samples C3-31, H87, A4, C6b, B1 from Brigatti *et al.*, 2000*b*; square: samples from Redhammer and Roth, 2002). Mean standard deviation on the $A-$O4 distance and $M2-\hat{O}4-M2$ angle is reported by the error bar in the bottom-right of each plot.

reduced with increasing F and oxy-substitutions for OH.

Another effect associated with the same crystal-chemical mechanism occurs in the octahedral sites; the angles formed by [001] with $M1-$O4 and $M2-$O4 bonds [$M2-O4_{[001]}$] vary as a function of F content (Fig. 1*c*).

Figure 1*d* introduces the variation of the angle defined by the octahedral position $M2$, the anionic position O4 and the other symmetry-dependent $M2$ cation $M2-\hat{O}4-M2$. This angle, which is also observed to decrease with tetrahedral Si content and to increase with octahedral Al content, reflects structural modification associated with $A-$O4 distance, which increases with the angle and decreases with the octahedral thickness, as expected. Consequently the F-for-OH substitution, which directly leads to a decrease in the $A-$O4 distance (Fig. 1*b*) is also connected to an increase in octahedral thickness, which is inversely related to $A-$O4 (Fig. 2*a*). This latter effect is consistent with the limited Al content observed in fluorannite and annite, with respect to the annite crystals from peraluminous granites used for comparison. Also the variance of

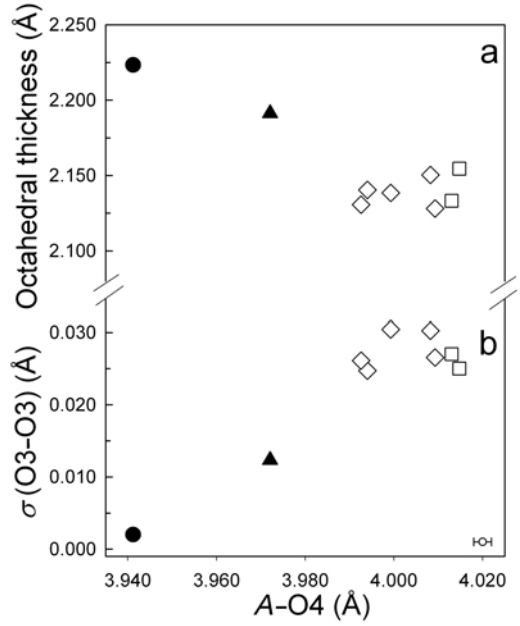

FIG. 2. Relationship between (*a*) the octahedral thickness and (*b*) the variance of $O3-O3$ octahedral edges ($\sigma O3-O3$) with $A-$O4 distance. Symbols and samples as in Fig. 1. Mean standard deviation on $A-$O4 distance is reported (see bottom-right of diagram).

octahedral unshared edges [σ(O3−O3)], directly related to *A*−O4 (Fig. 2*b*), reflects octahedral heterovalent substitutions (Brigatti and Guggenheim, 2002) and, in our case, mostly Li, Fe^{3+} and Al^{3+} octahedral contents. Octahedral chemistry plays a significant role in determining octahedral and interlayer structural parameters. In particular, the octahedral Al content could be related to the variance of the distances between the octahedral cations and oxygen atoms [σ(*M*−O)], with a positive correlation. This evidence further emphasizes the homo-octahedral character of fluorannite, which is octahedral-Al free.

Another effect, involving the tetrahedral site, is an observed positive correlation of tetrahedral-cation–basal-oxygen-atom distance, projected normal to (001) [*T*−O1⊥(001)], with F content. On the contrary, the trend with tetrahedral-cation–apical-oxygen-atom [*T*−O3⊥(001)], is inverse (Fig. 3*a*,*b*).

All the observed trends confirm the influence of F content on the overall layer topology, with particular significance for the structural parameters measured along [001]. Furthermore, F, as previously observed, seems to effectively stabilize the trioctahedral structure of the mica, as confirmed by the almost-complete homo-octahedral character of fluorannite, as well as promote populations of large octahedral cations, consistently with an increase in octahedral thickness.

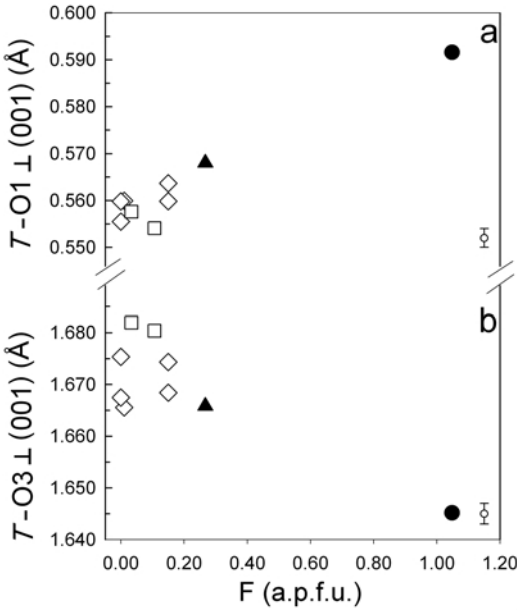

FIG. 3. Variation of the tetrahedral distances (*a*) *T*−O1 and (*b*) *T*−O3 normal to (001) with *A*−O4. Symbols and samples as in Fig. 1.

Acknowledgements

The authors thank R. Pagano and D. Kile who kindly supplied the fluorannite and annite samples. This work was significantly improved after the constructive suggestions of the two referees, G. Cruciani and G. Redhammer, as well as Principal Editor, M. Welch. This study was financially supported by the Ministero dell'Università e della Ricerca Scientifica of Italy (MIUR PRIN2006).

References

Boukili, B., Robert, J.-L., Bény, J.-M. and Holtz, F. (2001) Structural effects of OH-F substitution in trioctahedral micas of the system: K_2O-FeO-Fe_2O_3-Al_2O_3-SiO_2-H_2O-HF. *Schweizerische Mineralogische und Petrographische Mitteilungen*, **81**, 55−67.

Boukili, B., Holtz, F., Bény, J.-M. and Robert, J.-L. (2002) Fe-F and Al-F avoidance rule in ferrous-aluminous (OH,F) biotites. *Schweizerische Mineralogische und Petrographische Mitteilungen*, **82**, 549−559.

Brigatti, M.F. and Guggenheim, S. (2002) Mica crystal chemistry and the influence of pressure, temperature and solid solution on atomistic models. Pp. 1−98 in: *Micas: Crystal Chemistry and Metamorphic Petrology* (A. Mottana, F.P. Sassi, J.B. Thompson Jr. and S. Guggenheim, editors). Reviews in Mineralogy and Geochemistry **46**, Mineralogical Society of America, Washington D.C.

Brigatti, M.F., Lugli, C., Poppi, L., Foord, E.E. and Kile, D. (2000*a*) Crystal chemical variations in Li- and Fe-rich micas from Pikes Peak batholith (central Colorado). *American Mineralogist*, **85**, 1275−1286.

Brigatti, M.F., Frigieri, P., Ghezzo, C. and Poppi, L. (2000*b*) Crystal chemistry of Al-rich biotites coexisting with muscovites in peraluminous granites. *American Mineralogist*, **85**, 436−448.

Bruker (2003*a*) *APEX2*. Bruker AXS Inc., Madison, Wisconsin, USA.

Bruker (2003*b*) *SAINT-IRIX*. Bruker AXS Inc., Madison, Wisconsin, USA.

Comodi, P., Zanazzi, P.F., Weiss, Z., Rieder, M. and Drabek, M. (1999) 'Cs-tetra-ferri- annite': high-pressure and high-temperature behavior of a potential nuclear waste disposal phase. *American Mineralogist*, **84**, 325−332.

Comodi, P., Drabek, M., Montagnoli, M., Rieder, M.,

Weiss, Z. and Zanazzi, P.F. (2003) Pressure-induced phase transition in synthetic trioctahedral Rb-mica. *Physics and Chemistry of Minerals*, **30**, 198–205.

Donnay, G., Morimoto, N., Takeda, H. and Donnay, J.D.H. (1964) Trioctahedral one-layer micas. 1. Crystal structure of a synthetic iron mica. *Acta Crystallographica*, **17**, 1369–1373.

Donovan, J.J. (1995) *PROBE: PC-based data acquisition and processing for electron microprobes*. Advanced Microbeam, Vienna, Ohio, USA.

Fechtelkord, M., Behrens, H., Holtz, F., Bretherton, J.L., Fyfe, C.A., Groat, L.A. and Raudsepp, M. (2003*a*) Influence of F content on the composition of Al-rich synthetic phlogopite: Part I. New information on structure and phase-formation from ^{29}Si, ^{1}H, and ^{19}F MAS NMR spectroscopies. *American Mineralogist*, **88**, 47–53.

Fechtelkord, M., Behrens, H., Holtz, F., Bretherton, J.L., Fyfe, C.A., Groat, L.A. and Raudsepp, M. (2003*b*) Influence of F content on the composition of Al-rich synthetic phlogopite: Part II. Probing the structural arrangement of aluminum in tetrahedral and octahedral layers by ^{27}Al MQMAS and ^{1}H/^{19}F-^{27}Al HETCOR and REDOR experiments. *American Mineralogist*, **88**, 1046–1054.

Gianfagna, A., Scordari, F., Mazziotti-Tagliani, S., Ventruti, G. and Ottolini, L. (2007) Fluorophlogopite from Biancavilla (Mt. Etna, Sicily, Italy): Crystal structure and crystal chemistry of a new F-dominant analog of phlogopite. *American Mineralogist*, **92**, 1601–1609.

Hawthorne, F.C., Ungaretti, L. and Oberti, R. (1995) Site populations in minerals: terminology and presentation of results. *The Canadian Mineralogist*, **33**, 907–911.

Kremenetsky, A.A., Beskin, S.M., Lehmann, B. and Seltmann, R. (2000) Economic geology of granite-related ore deposits of Russia and other FSU countries; an overview. Pp. 3–56 in: *Ore-bearing Granites of Russia and Adjacent Countries* (A. Kremenetsky, B. Lehmann, R. Seltmann, editor). IAGOD Monograph Series, IMGRE, Moscow.

Lalonde, A.E., Rancourt, D.G. and Chao, G.Y. (1996) Fe-bearing trioctahedral micas from Mont Saint-Hilaire, Quebec, Canada. *Mineralogical Magazine*, **60**, 447–460.

Mason, R.A. (1992) Models of order and iron-fluorine avoidance in biotite. *The Canadian Mineralogist*, **30**, 343–354.

Mellini, M., Weiss, Z., Rieder, M. and Drabek, M. (1996) Cs-ferriannite as a possible host for waste cesium; crystal structure and synthesis. *European Journal of Mineralogy*, **8**, 1265–1271.

Munoz, J.L. (1984) F-OH and Cl-OH exchange in micas with applications to hydrothermal ore deposits. Pp. 469–493 in: *Micas* (S.W. Bailey, editor). Reviews in Mineralogy, **13**, Mineralogical Society of America, Washington, D.C.

Papin, A., Sergent, J. and Robert, J.-L. (1997) Intersite OH-F distribution in an Al-rich synthetic phlogopite. *European Journal of Mineralogy*, **9**, 501–508.

Redhammer, G.J. and Roth, G. (2002) Single-crystal structure refinement and crystal chemistry of synthetic trioctahedral micas $KM_3(Al^{3+},Si^{4+})_4O_{10}(OH)_2$, where M = Ni^{2+}, Mg^{2+}, Co^{2+}, Fe^{2+} or Al^{3+}. *American Mineralogist*, **87**, 1464–1476.

Redhammer, G.J. and Roth, G. (2004) The ferriannite $KFe^{2+}{}_3(Al_{0.26}Fe^{3+}{}_{0.76}Si_3)O_{10}(OH)_2$ at 100 and 270 K. *Acta Crystallographica,* **C60**, 33–36.

Robert, J.-L., Bény, J.-M., Della Ventura, G. and Hardy, M. (1993) Fluorine in micas: crystal-chemical control of the hydroxyl-fluorine distribution between trioctahedral and dioctahedral sites. *European Journal of Mineralogy*, **5**, 7–18.

Sheldrick, G.M. (1997) *SHELX-97; a program for crystal structure determination*. University of Göttingen, Germany.

Sheldrick, G.M. (2003) *SADABS*. University of Göttingen, Germany.

Shen, G. (2002) Suzhou fluorannite-rich granite: differentiation remnant of F-rich A-type granitic magma. *Huanan Dizhi Yu Kuangchan*, **2**, 50–57 (in Chinese).

Shen, G., Lu, Q. and Xu, J. (2000) Fluorannite: a new mineral of the mica group from the western suburb of Suzhou, Zhejiang Province, China. *Yanshi Kuangwuxue Zazhi*, **19**, 355–362 (in Chinese with English abstract).

Shen, Q., Li, Z., Wu, Z. and Lu, A. (2002) The Mössbauer spectrum of the new mineral fluorannite. *European Journal of Mineralogy*, **14**, 1049–1052.

Signorelli, S., Vaggelli, G. and Romano, C. (1999) Pre-eruptive volatile (H_2O, F, Cl and S) contents of phonolitic magmas feeding the 3550 year old Avellino eruption from Vesuvius, southern Italy. *Journal of Volcanology and Geothermal Research*, **93**, 237–256.

Solodov, N.A., Semenov, E.I. and Burkov, V.V. (1987) *Geological Reference Book on Heavy Lithophile Rare Metals*. Nedra, Moscow, 439 pp (in Russian).